In Situ WAXS/SAXS Structural Evolution Study During Uniaxial Stretching of Poly(ethylene terephthalate) Nanocomposites in the Solid State: Poly(ethylene terephthalate)/Titanium Dioxide and Poly(ethylene terephthalate)/Silica Nanocomposites

Lyudmil V. Todorov, Carla I. Martins, Júlio C. Viana

Institute for Polymers and Composites/I3N, Department of Polymer Engineering, University of Minho, Guimarães 4800-058, Portugal
Correspondence to: J. C. Viana (E-mail: jcv@dep.uminho.pt)

ABSTRACT: This work reports an *in situ* WAXS and SAXS investigation, under X-ray synchrotron source radiation, on the structural evolution during solid-state uniaxial deformation of poly(ethylene terephthalate) (PET) nanocomposites with 0.3 wt % of 3D nanoparticles [nanotitanium dioxide (TiO_2) and nanosilica (SiO_2)]. Good dispersion and average agglomerate sizes of nanoparticles of about 80 nm for both nanocomposites were revealed by transmission electron microscopic characterization. The influence of the nanofillers on the deformation-induced phase's formation and their evolution along the stretching process were compared with respect to the neat PET. WAXS results indicated that the structural evolution of all samples passes through three main stages, with evolution of amorphous phase into mesophase, a rapid increase of molecular orientation, and the formation of a periodical mesophase (PM). The incorporation of the nanofillers promoted a higher fraction, and an earlier formation, of PM during stretching when compared with pure PET. Furthermore, the presence of TiO_2 nanoparticles in the PET matrix resulted in the earliest formation and the highest amount of PM and the retardation of crack growth and bigger voids when compared with PET/SiO_2 nanocomposite. A multiscale structural evolution mechanism is proposed to interpret these results. © 2013 Wiley Periodicals, Inc. J. Appl. Polym. Sci. 000: 000–000, 2013

INTRODUCTION

Nowadays, one of the most widely used materials for plastic packaging is poly(ethylene terephthalate) (PET) because of its enhanced mechanical, thermal, and barrier properties. An alternative for performance improvement of PET, generally consisting of the enhancement of mechanical, thermal, and barrier properties, is the reinforcement of neat polymer matrix with different inorganic nanoparticles, that is, PET nanocomposites. PET can be reinforced with three main types of nanofillers, depending on the number of dimensions on the nanometer scale, namely, (i) 1D, with one dimension (e.g., nanoclays), (ii) 2D, with two dimensions (e.g., carbon nanotubes), and (iii) 3D, with three dimensions, usually with spherical-like shape [e.g., nanosilica (SiO_2) and nanotitanium dioxide (TiO_2)].[1]

Recently, specific interest was devoted to PET/3D nanocomposites, in particular PET/TiO_2[2–5] and PET/SiO_2,[5–15] obtained via various preparation methods. Incorporation of isodimensional

TiO_2 nanoparticles into PET matrix was carried out via (i) *in situ* polymerization,[3] (ii) solvent-assisted,[2] and (iii) melt-blending[4] techniques. Much more interest was received for SiO_2 as nanoreinforcement for PET when compared with TiO_2. For PET/SiO_2 nanocomposites, preparation methods used are as follows: (i) *in situ* polymerization,[6,7,10–12] (ii) solvent-assisted,[2] (iii) melt-blending,[4,13] and (iv) cryomilling-blending techniques.[14,15] Among all the compounding methods, the melt-blending technique was recognized as the most suitable for commercial scale-up production.[16] Enhanced mechanical performance, in comparison with neat PET, was reported for PET/TiO_2 and PET/SiO_2 nanocomposites that were prepared via melt-blending techniques, that is, increment of (i) elastic modulus,[4,5,12,13] (ii) yield stress,[5] (iii) maximum stress,[4] and (iv) deformation capability.[12,13]

The understanding of the mechanisms underlying these enhancements, as well as the effect of inorganic nanofillers on the structural evolution, is crucial for the successful application

of polymer nanocomposites. In this regard, a very few attempts have been made to study those in detail. Kim and Michler[17,18] studied the toughening mechanisms occurring in semicrystalline polymer nanocomposites by several electron microscopic techniques. On the basis of these investigations, they proposed three stages of deformation mechanisms for nanocomposites with spherical nanofillers, namely, (i) Stage I, where the nanoparticles agglomerates act as a stress concentrators because of their different elastic properties that leads to agglomerates dilatation; (ii) Stage II, because of stress concentration, voids formation through debonding occurs within the agglomerates; and (iii) Stage III, once the voids have occurred, corresponding to an increase in the shear stress component, as a consequence, further shear yielding is greatly induced in the matrix. Reynaud et al.[19] investigated the effect of SiO_2 nanoparticle size and suggested that (i) smaller nanoparticles gather into smaller aggregates that leads to a multiple debonding process, leading to multiple voids with dimensions similar to the particle, size and (ii) bigger nanoparticles form bigger aggregates, undergoing a single debonding process, causing bigger size voids.[17,18] It is also well known,[20–22] grounded on the time-resolved SAXS investigations, that the uniaxial stretching in solid state of amorphous polymers is accompanied by a substantial structural damage that occurs by voids nucleation and propagation. Macroscopically, this is revealed by the whitening of the specimen on deformation.

To improve and control the ultimate mechanical properties for a wide range of applications and, in particular, to optimize the stiffness/toughness balance, a better understanding of the interrelationships between nanoparticles and structural evolution during deformation processes is clearly required. In this regard, this work aims on revealing the effect of incorporated different 3D nanoparticles, that is, TiO_2 and SiO_2, into PET polymer matrix on the structural evolution and deformation mechanism during the uniaxial stretching in the solid state.

EXPERIMENTAL

Materials
In this work the following materials were used:

- PET with intrinsic viscosity of 0.74 ± 0.02 dl g^{-1} (bottle grade) as polymer matrix, provided by Tergal Fibers S.A., France.
- 3D nanoreinforcements with spherical-like shape (i) TiO_2 (AEROXIDE TiO_2 P25) consists of 80% anatase and 20% rutile with specific surface according to BET 50 ± 15 m^2 g^{-1}, and (ii) SiO_2 (AEROSIL 200) with specific surface according to BET 200 ± 25 m^2 g^{-1}; these specifications are given in Table I according to the supplier's data (Degussa AG, Germany).

Sample Preparation
Samples used in this work were produced via direct melt blending of PET with 0.3 wt % of TiO_2 and SiO_2 nanoparticles using an asymmetric batch minimixer according to the experimental procedure described in our previous works.[23] After blending, compression-molded samples were prepared and cooled down very rapidly on a water recipient at 5°C to obtain amorphous

Table I. Characterization of the Morphologies of PET Nanocomposites

Nanofiller	D_{av}[a] (nm) Agglomerates[a]	Particles[a]	D_{av}[b] (nm) Composite
TiO_2	100	≈ 21	88 ± 58
SiO_2	100	≈ 12	87 ± 60

[a] D_{av}, main average diameter as a powder (according to supplier's data).
[b] D_{av}, average agglomerate diameter as calculated by eq. (1).

PET plaques. These plaques were then cut with a curved axisymmetric shape (length 35 mm, minimum cross section 13.9 mm × 0.3 mm, length of 14 mm, and curvature radius of 10.44 mm) and used for the *in situ* WAXS and SAXS simultaneous to the uniaxial tensile testes.

Transmission Electron Microscope
Agglomerate sizes of the particles were obtained using transmission electron micrographs (TEM) taken from ultramicrotome cuts with ~ 60 nm of thickness, made through the thickness of the compression-molded samples. For this, a JEOL JEM 1010 at a voltage of 100 kV was used. Three micrographs per nanocomposite were used for particle agglomerate measurements from randomly transversal cuts. 3D nanoparticle agglomerates incorporated into PET nanocomposites were assumed to be elliptical. The average agglomerate diameter, D_{av}, was calculated as follows:

$$D_{av} = \frac{\sum_{i=1}^{n}[(d_1+d_2)_i/2]}{n}, \qquad (1)$$

where d_1 and d_2 are the main diameters of each agglomerate, and n is the number of agglomerates considered (at least five particle measurements were considered).

Simultaneous Deformation and *In Situ* Synchrotron Characterization
Uniaxial continuous stretching in the solid state (at 23°C) and *in situ* WAXS and SAXS characterization were performed simultaneously. WAXS and SAXS were carried out under synchrotron radiation [Ge (111) and $\lambda = 0.15$ nm] at HASYLAB, DESY, Hamburg (A2 beamline). The mechanical testing was performed on a homemade uniaxial tensile stretching device enabling to move both grips in opposed directions so that the X-ray beam is maintained at the center of the sample during the stretching procedure. Stretching apparatus output, the force and displacement curve was converted into homogeneous stress–strain curves (σ_N vs. ln λ). It was assumed that the curved axisymmetric tensile specimen deforms through a rectangular neck. The stretching ratio, λ, was defined as follows:

$$\lambda = \frac{l}{l_0}, \qquad (2)$$

where l is actual tensile specimen length and l_0 is the grip distance. The homogeneous stress was calculated as follows:

$$\sigma_N = \frac{F}{A_0} \lambda , \qquad (3)$$

where F is the force and A_0 is the initial minimum tensile specimen cross-sectional area.

The specimens were mounted perpendicular to the incident X-ray beam and stretched in the vertical direction. Background scattering was subtracted, and all plots were normalized with respect to the incident X-ray intensity, accumulation time, and specimen thickness (assuming a homogeneous deformation[24]). Equipmental setups were as follows:

i. WAXS: Sample-to-detector distance of 145 mm and 2D WAXS patterns were acquired with accumulation time of 20 s. Samples were stretched at a constant cross-head velocity of 2 mm min^{-1} (strain rate of 0.002 s^{-1}). Such accumulation time was set as a lowest as possible for considered strain rate.[25–27] WAXS was calibrated by means of a crystalline PET sample.

ii. SAXS: Sample-to-detector distance of 3025 mm and 2D SAXS patterns were acquired with accumulation time of 30 s. Samples were stretched at a constant cross-head velocity of 5 mm min^{-1} (strain rate of 0.006 s^{-1}).

Mass Fractions of the Phase. The two linear intensity profiles, taken along the equatorial and meridional directions from the 2D WAXD patterns, were used to estimate mass fractions of amorphous, mesophase, and periodical mesophase (PM). A peak-fitting program was used to deconvolute the peaks of the distinct phases that were fitted by a Gaussian function. The morphology of the studied samples was assumed to consist of two phases[5,28]: (i) amorphous—isotropic phase and (ii) mesophase—anisotropic phase, with degree of packing and order between the crystalline and the amorphous phase. The amount of amorphous phase was assumed to be proportional to the area of the peak taken from the meridional profile. The subtraction of the amorphous fraction from the total area of the peak taken in the equatorial profile was proportional to the amount of the mesophase. The mass fractions of the individual phases were taken as the ratio of the area for each phase to the total area of the equatorial profile. As the strain increases, the WAXS patterns can exhibit a pair of meridional mesomorphic reflection (10$\bar{3}$) at about $2\theta = 25.8°$,[29,30] indicating conformational regularity, and called PM.[26,31] At this stage of deformation, the morphologies of the samples were considered to be composed of three phases: (i) amorphous, (ii) mesophase, and (iii) PM, mesophase with conformational periodicity perpendicular to the stretching direction. The area of fitted (10$\bar{3}$) peak profile was used to determine the mass fraction of the PM. The sum of the area convoluted under the equatorial intensity profile and the meridional (10$\bar{3}$) peak was assumed to be the total area. The mass fractions of the individual phases were taken as the ratio of the area for each phase to the total area.

Average Polymer Orientation. The WAXS patterns were integrated along an azimuthal angle of $\phi = 0 - \pi/2$ ($\phi = 0$ at equator), over a section with width of $2\theta = 13°–28°$, to calculate the average polymer orientation, f_{av}. The sector encloses all possible crystal reflections of crystallographic planes, isotropic amorphous phase, and mesophases of PET.[32] The Hermans' orientation function was used to evaluate the average polymer orientation, f_{av}, which is calculated as follows[33]:

$$f_{av} = \frac{3\langle\cos^2\varphi\rangle - 1}{2}, \qquad (4)$$

where the $\langle\cos^2\varphi\rangle$ is defined as follows:

$$\langle\cos^2\varphi\rangle = \frac{\int_0^{\pi/2} I(\varphi)\cos^2\varphi\sin\varphi\,d\varphi}{\int_0^{\pi/2} I(\varphi)\sin\varphi\,d\varphi}, \qquad (5)$$

where ϕ is the azimuthal angle, I is the diffracted intensity, and $\langle\cos^2\phi\rangle$ is the average angle that the normal makes with the principal deformation direction.

RESULTS AND DISCUSSION

Morphology of the Nanocomposites

TEM investigations showed relatively good dispersion of the nanofillers into the polymer matrix for both nanocomposites.[23] Average agglomerates diameter measured from TEM images, listed in Table I, revealed that the agglomerates of the each nanofiller were slightly reduced, by melt-blending processing, when compared with the initial powder size. PET/TiO$_2$ and PET/SiO$_2$ morphologies are depicted in Figure 1 and reported elsewhere.[23]

Structural Evolution by WAXS

Figure 2 presents the homogenous stress–strain curves obtained during the uniaxial stretching and selected 2D WAXS patterns of PET/TiO$_2$ and PET/SiO$_2$ nanocomposites (arrows indicate the strains where patterns were acquired). Both specimens show similar evolution of the 2D WAXS patterns and a yielding point at equal strain (ln λ = 0.05). Both nanocomposites, despite the different nanofillers, have similar neck evolution during the stretching, as depicted in Figure 3. From load application till strain of about ln λ = 0.2, the 2D WAXS patters are characterized by an amorphous halo, which slightly intensifies in this interval of stretching. This part of stretching corresponds to the region of strain–stress curve that includes the elastic deformation and yielding regimes, where necking initiates near the middle of tensile bar, as shown in Figure 3(b and g), but outside the measured X-ray area. In fact, the neck forms out of the sample center where the WAXS investigation was carried out [see Figure 3(c and h)]. As the strain of ln λ = 0.2 till sample brakeage, both PET/3D nanocomposites 2D WAXS patterns are characterized by two diffused spots at the equator, indicative of considerable polymer chains orientation into the stretching direction[34–38] and a distinctive meridional (10$\bar{3}$) reflection that is attributed to PM.[29,30] This is connected to the neck propagation through the examined region of the sample [Figure 3(d and i)].

The equatorial and meridional intensity versus 2θ profiles extracted from the 2D WAXS patterns, for both samples, are depicted in Figure 4. Distinct amorphous PET equatorial reflection peaks, at about $2\theta \approx 19°$, might be identified for both nanocomposites at lower stain level [up to ln λ = 0.2; Figure 4(a,c)]. This peak intensifies with stretching and shifts to the
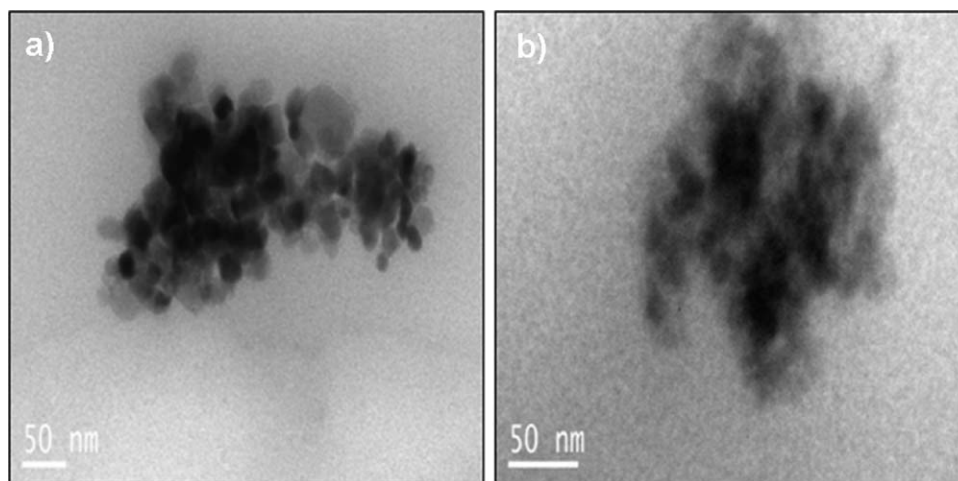
Figure 1. TEM micrographs of (a) PET/TiO₂ and (b) PET/SiO₂ nanocomposites.[23]

angle of $2\theta \approx 21°$ at the ultimate strains. In meridional profiles Figure 4(b,d) isotropic (amorphous) meridional peaks at $2\theta = 19°$ are initially observed, which shift to lower diffraction angles at lower stretching levels. At strain of $\ln \lambda = 0.2$, the mesomorphic peak $(10\overline{3})$ emerges at about $2\theta \approx 26°$, which increases in intensity with strain till sample breakage. Simultaneously, the equatorial amorphous peak narrows without significant angular position change. However, at strain of $\ln \lambda = 0.2$, the PET/SiO₂ samples show a weak $(10\overline{3})$ peak, evidencing a small amount of PM formation, in contrast to the PET/TiO₂ sample $(10\overline{3})$ peak that is more intense corresponding to a greater content of this phase.

Phases and average polymer orientation evolutions with strain for both nanocomposites pass through similar pathways, as shown in Figure 5. Based on the average polymer orientation curve shape, three main stages can be identified. In the first stage, Stage I, the average polymer orientation remains almost constant as the strain increases up to $\ln \lambda = 0.08$. Suddenly, there is a fast increase of the average polymer orientation, from around $f_{av} = -0.2$ up to $f_{av} = 0.6$, in a short interval of strain, between $0.08 < \ln \lambda < 0.3$, which corresponds to Stage II. Hereafter, at strain of $\ln \lambda = 0.3$, starts Stage III where a plateau on the maximum orientation is reached and is maintained till the end of the deformation process.
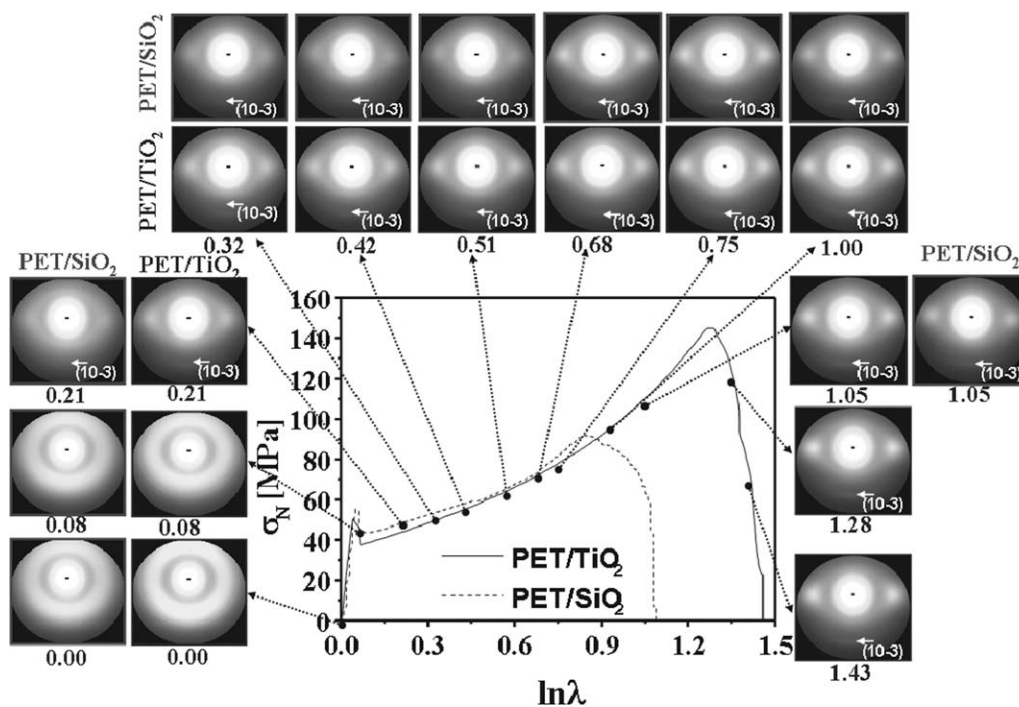

Figure 2. Homogeneous stress–strain curves of PET/TiO₂ and PET/SiO₂ nanocomposites and selected 2D WAXS patterns obtained in the solid state (23°C).
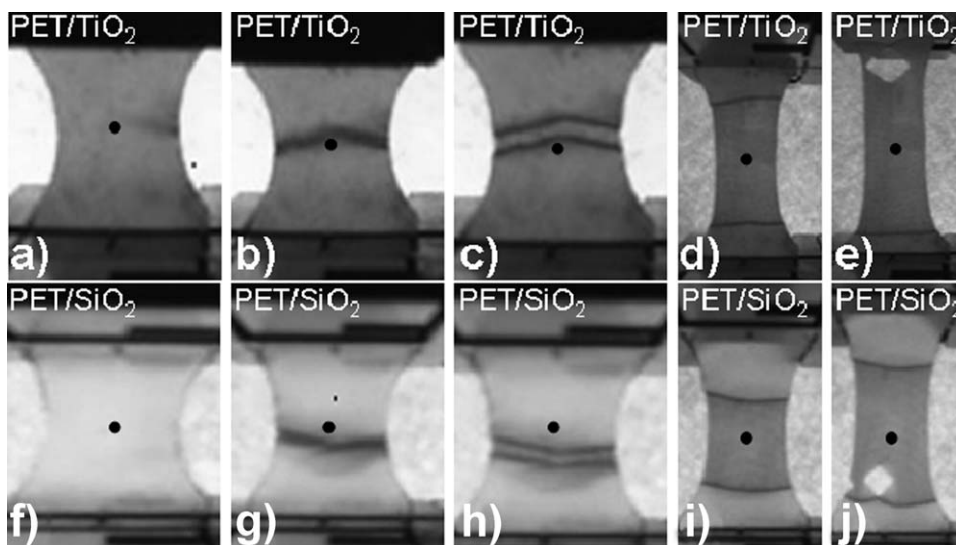
Figure 3. *In situ* video images of PET/TiO$_2$ and PET/SiO$_2$ nanocomposites during deformation: (a and f) start of deformation; (b and g) neck initiation; (c and h) neck formation; (d and i) neck propagation; and (e and j) sample rupture obtained in the solid state (23°C; the black spot represents approximately the X-ray beam incident point).
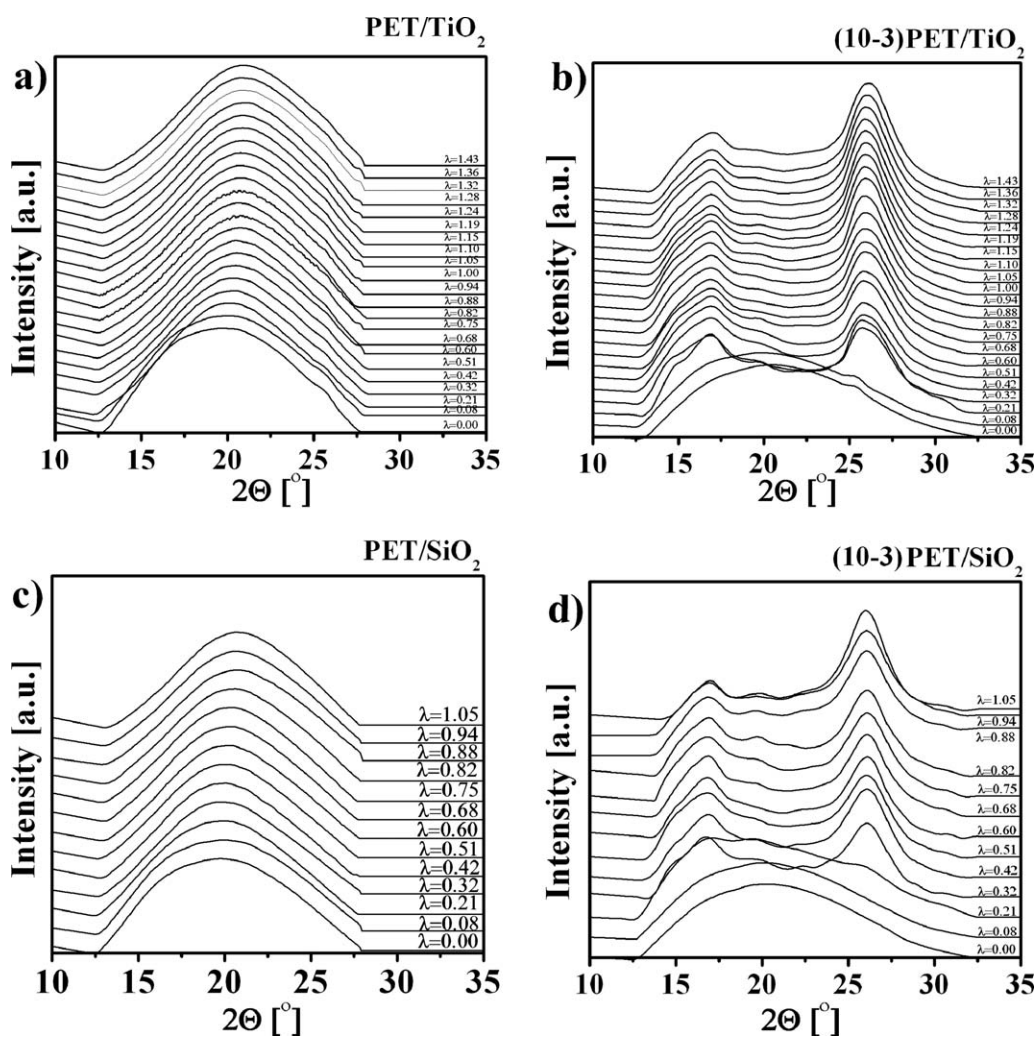

Figure 4. Linear intensity profiles extracted from 2D WAXS patterns: (a) equatorial and (b) meridional profiles of PET/TiO$_2$ nanocomposite; and (c) equatorial and (d) meridional profiles of PET/SiO$_2$ nanocomposite, all obtained in the solid state (23°C).
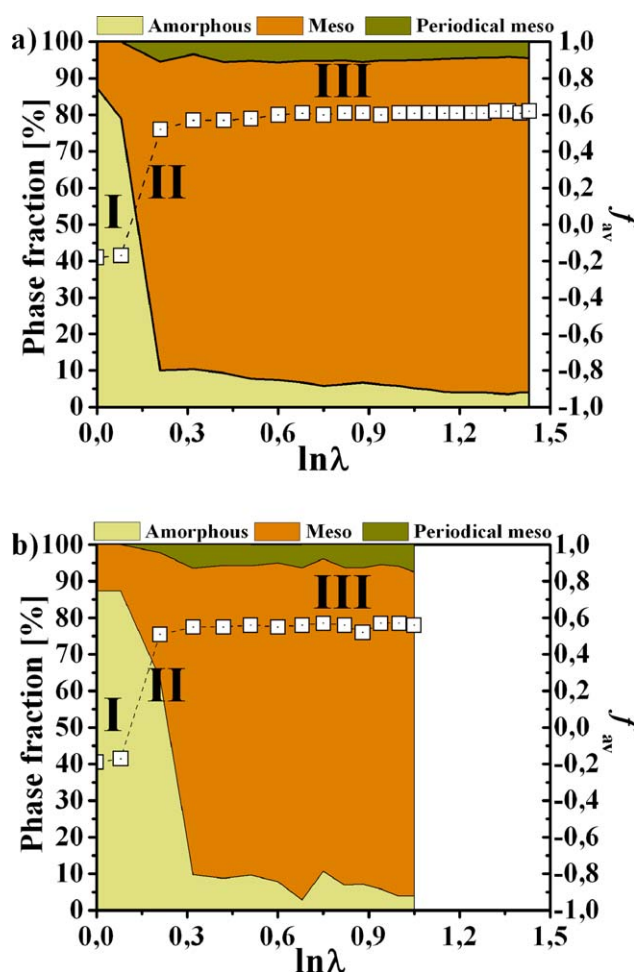
Figure 5. Phase fraction and average polymer orientation, f_{av}, evolution obtained in the solid state (23°C) of (a) PET/TiO$_2$ and (b) PET/SiO$_2$ nanocomposites. [Color figure can be viewed in the online issue, which is available at wileyonlinelibrary.com.]

The evolution of phase by stages can be described as follows:

- Stage I: This stage is characterized by a slight decrement of amorphous phase due to its transformation into more organized mesophase.
- Stage II: This stage is characterized by a sharp increment of mesophase due to consumption of amorphous phase, together with the indication of PM formation.
- Stage III: This stage features modest transformation of amorphous phase into mesophase with strain, at almost constant maximum PM content.

Both nanocomposites are characterized by an initial equal fraction of mesophase, about 12%. Nevertheless, some dissimilarity between the PET/3D nanocomposites evolution can be noted. The presence of TiO$_2$ nanoparticles in the PET matrix promoted the increment of mesophase by 10%, during Stage I, whereas the PET/SiO$_2$ does not alter this fraction. PET/TiO$_2$ samples also achieved the maximum PM content at the middle (ln λ = 0.2) of Stage II, whereas nanocomposite reinforced with SiO$_2$ only at the end (ln λ = 0.3) of Stage II. In contrast, both sam-

ples fail at dissimilar strain, but with similar phase fractions content of mesophase and amorphous phase, 90% and 4%, respectively, whereas the PM content in both phases is different: for PET/TiO$_2$ specimen it is of 7% and 4% in case of PET/SiO$_2$. Such difference might be related to the different nature of nanofillers and its effect on the material morphology, leading to unlike deformation capability of PET nanocomposites.

The structural evolution of PET/3D nanocomposites as detected by WAXS investigation can be summarized as follows:

- Stage I is related to the neck initiation and formation of specimen central area that leads to an amorphous halo in the 2D WAXS patterns centered at about $2\theta \approx 19°$ and presented in both equatorial and meridional intensity profiles, and no change on the average polymer orientation. In this stage, there is a slight increment of the mesophase fraction due to amorphous phase consumption.
- Further stretching leads to the beginning of Stage II that is associated with neck propagation on the tensile bar over the X-ray incident point; the average polymer orientation rapidly rises in the stretching direction, which it translates into two spots at the equator and a reflection $(10\bar{3})$ at meridional of the 2D WAXS patterns. Although the I–2θ linear equatorial profiles featured intensified and concentrated peak at about $2\theta \approx 20°$, the meridional profile shows an amorphous peak at $2\theta \approx 16°$, together with a PM peak at about $2\theta \approx 26°$. During Stage II, the increment of polymer chains orientation leads to a fast transformation of amorphous phase into mesophase, together with the nucleation of a small amount of PM from an oriented mesophase portion.
- At end of Stage II, starts Stage III with the achievement of a plateau of polymer orientation level that is descriptive for network extensibility limits attainment. This stage ends with sample rupture, and a typical stable necking propagation is observed. The level-off of molecular orientation is concomitant with equatorial spots and meridional reflection $(10\bar{3})$ intensification with strain in the 2D WAXS patterns, which is translated into slight shifts to higher angles of the equatorial and isotropic meridional peaks, whereas the $(10\bar{3})$ meridional peak intensifies without change of its position. On the other hand, the PM content remains constant throughout this stage, and the mesophase content increases somewhat due to the decrement of the amorphous phase. Tensile bar rupture occurs as a result of macroscopic cracks happening along the necked zone [as shown in Figure 3(e and j)].[39]

The effect of incorporation of TiO$_2$ and SiO$_2$ nanoparticles into the PET matrix on the structural evolution when compared with the neat PET[31] is shortened hereafter. The presence of nanofillers leads to higher strain levels during the plastic deformation of the matrix and enhanced its toughness. Both nanocomposites show a yield point at ln λ = 0.05, and the neat PET at ln λ = 0.04. Initially, the 3D nanocomposites, regardless of the nanofillers nature, have identical amount of mesophase of about 12%, which is about four times higher than the neat PET (i.e., 3%) due to the nucleation effect of the nanofillers.[23] The PET nanocomposites, regardless of their nanofiller type, promoted in relation to the PET samples:
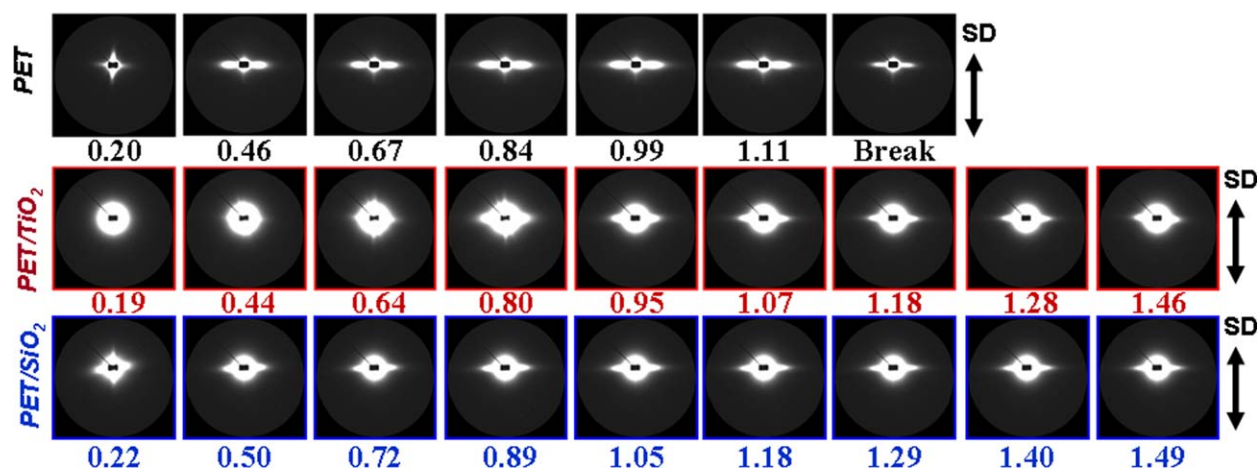
Figure 6. Selected 2D SAXS patterns and corresponding homogeneous strain, ln λ, obtained during the *in situ* SAXS characterization in the solid state (23°C). [Color figure can be viewed in the online issue, which is available at wileyonlinelibrary.com.]

i. an earlier periodical phase formation in Stage II, and
ii. improved the amount of mesophase and consequently about four times greater maximum PM content during Stage III.

On the other hand, the incorporation of TiO$_2$ nanoparticles promoted greater PM content, when compared with the SiO$_2$ nanoparticles.

Structural Evolution by SAXS

Figure 6 shows selected 2D SAXS patterns of neat PET and its nanocomposites obtained during the plastic deformation region after the yielding point. Based on the characteristic features occurring in 2D SAXS patterns during stretching, distinct differences can be denoted in the structural evolution due to dissimilar deformation mechanisms taking place.

First, 2D SAXS image of neat PET sample at ln λ = 0.2 shows a cross-shaped pattern. This pattern is representative of craze/void morphology, where the streak parallel to the loading direction is related to the total reflection at the craze/polymer interfaces, and the streak perpendicular to the loading direction is associated to the fibril/void scattering.[40] Crazes are typical of amorphous polymer during deformation and have been observed for neat PET[20–22] and for its nanocomposites.[41,42] The 2D SAXS patterns of neat PET at strain of ln λ = 0.46 evolve into a streak perpendicular to the loading direction that is presented till the samples breakage, caused by the fibril/void structural elongation into the stretching direction.[40,43]

At lower strain levels, certain dissimilarity in 2D SAXS patterns shape of both nanocomposites is observed. At a strain of about ln λ = 0.2, the SAXS image of PET/TiO$_2$ sample features a ring shape, indicative of an isotropic orientation of voids in the sample, originated by cavitation of polymer matrix, and/or of nanoparticles agglomerates debonding. Craze formation may also be present, as the cross-shaped reflection can be overlapped by the ring scattering of the voids. The cross-shape scattering that is suggestive for retardation of crazes widening and growth suppressing within the polymer bulk[42] might be traced up to a strain of ln λ = 0.8 into the PET/TiO$_2$ 2D SAXS patterns. As the strain of ln λ = 0.95 till break, SAXS images evolve into a

single streak perpendicular to the stretching direction representative for fibril/void structure of highly elongated crazes and voids.[41,42] Intensively, the streak size is reduced till sample breakage.

On the other hand, first 2D SAXS patterns of PET/SiO$_2$ specimen feature a cross-shaped scattering (Figure 6), which is associated to a craze/void morphology.[42] Furthermore, at strains greater than ln λ = 0.5, the individual streak perpendicular to the stretching direction can be traced in 2D SAXS patterns, originated by scattering of the elongated crazes and voids.

Equatorial streaks profile can be used for qualitative estimation of elongated void sizes, that is, streak height correspond to void's height and its length to the void's diameter.[40,43] Based on the qualitative analysis of 2D SAXS patterns evolution in Figure 6, it might be suggested that:

i. the addition of TiO$_2$ nanoparticles promote the retardation of the crazes widening and growth, when compared with neat PET samples and PET/SiO$_2$ nanocomposite; and
ii. all nanocomposite samples evolve by elongated voids with somewhat shorter height and smaller diameter than the pure PET sample, whereas the TiO$_2$ particles cause formation of voids with slightly bigger diameter and similar length when compared with the SiO$_2$ particles.[19]

Multiscale Structural Evolution Model

The focus of this study was to investigate the influence of different types of nanofillers with spherical shape on the structural evolution of PET nanocomposites during the uniaxial stretching, in particular the strain-induced structural development and its dependence on deformation mechanism. In addition, this work aimed at investigating the effect of different type and sizes of nanofillers on all abovementioned physical phenomena. In this regard, the multiscale structural model is proposed, as illustrated in Figure 7, to interpret the structural evolution during tensile deformation of PET/TiO$_2$ and PET/SiO$_2$ nanocomposites. In the model, the mechanical behavior and average polymer orientation are related to the structural changes in three stages:
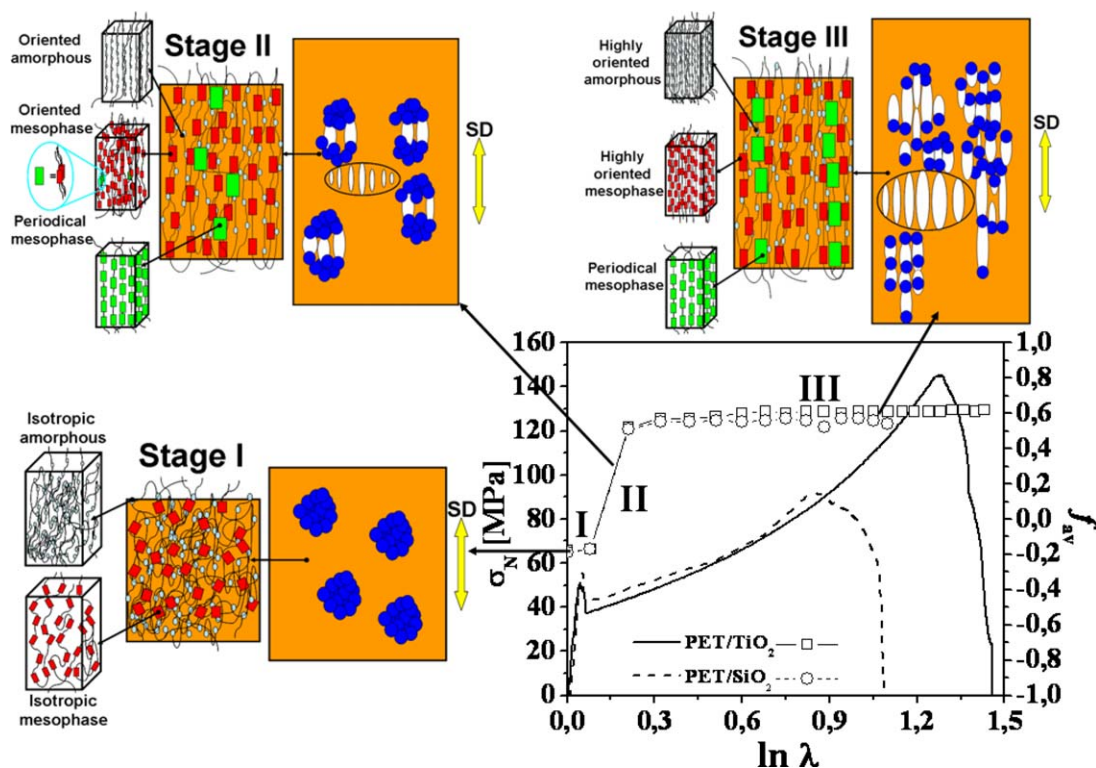
Figure 7. Schematic diagrams to illustrate the multiscale structural evolution during the solid state (23°C) and the uniaxial stretching of PET/3D (spherical) nanocomposites.

- Stage I: From the start of stretching till neck initiation, during which any variation of average polymer orientation is absent, a slight portion of amorphous phase evolves into mesophase. On the other hand, the inorganic agglomerates within the matrix become stress concentration centers.[17,18]
- Stage II: The beginning of this stage is associated with the neck formation. In a short interval of strain, crazes occur within the polymer matrix, and voids are formed inside the agglomerates via multiple debonding process.[17,18] The deformation volume is reduced, and polymer chains orient fast along the stretching direction. There is also a mesophase development from the oriented amorphous phase, and a small part of the oriented mesophase orders into PM. These sites may act as precursors of crystalline structures, if conditions are favorable.
- Then Stage III is initiated that lasts till sample failure, and it corresponds to sample lengthening through necking. During this stage, crazes within polymer bulk widen and lengthen with strain, causing individual fibrils rupture till those becomes microvoids, while the void originated by the debonding of agglomerates lengthens along the stretching direction. The polymer average orientation levels off at their maximum value, which is associated with the achievement of the chain extensibility limit, also forming a maximum PM fraction, which maintains constant up to samples breakage. With strain advancement, a small, highly oriented amorphous phase is transformed into mesophase, till tensile bar breaks.

CONCLUSIONS

Enhanced deformability and attained stress levels of nanocomposites with respect to neat PET were observed during deformation in solid state (23°C). The structural evolution of nanocomposites filled with 3D nanoparticles (0.3 wt % of TiO_2 and SiO_2) passes through three main stages:

i. Stage I: A small amount of amorphous phase evolves into mesophase at constant molecular orientation level (before necking occurs); the nanofillers agglomerates act as stress concentrators.
ii. Stage II: Neck zone formation; crazes within matrix and voids from debonding of nanoparticles agglomerates appear together with a rapid increase of polymer molecular orientation; sharp increment of mesophase at the reduction of the amorphous phase and the initiation of the formation of a PM from the mesophase;
iii. Stage III: Necking propagation; voids lengthen at a plateau of the average molecular orientation; the highest PM content is achieved, as well as a slight increment of mesophase.

Nanocomposites, regardless of the nanofiller type and with respect to neat polymer specimen, lead to improved amount of mesophase and greater content of maximum PM. TiO_2 nanofillers caused a slightly higher fraction of PM and its earlier formation than SiO_2. Crazes growth retardation is caused by the incorporation of TiO_2 nanoparticles when compared with PET and PET/SiO_2 samples. Nanocomposites form elongated voids with somewhat shorter height and smaller diameter than the

neat PET, whereas the TiO_2 particles originated the formation of wider voids but with similar length than the SiO_2 particles.

REFERENCES

1. Ray, S. S.; Okamoto, M., *Prog. Polym. Sci. (Oxford)* **2003**, *28*, 1539.

2. Fray, E.; Boccaccini, M.; Aldo, R., *Mater. Lett.* **2005**, *59*, 2300.

3. Han, K.; Yu, M., *J. Appl. Polym. Sci.* **2006**, *100*, 1588.

4. Taniguchi, A.; Cakmak, M., *Polymer* **2004**, *45*, 6647.

5. Todorov, L. V.; Viana, J. C., *J. Appl. Polym. Sci.* **2007**, *106*, 1659.

6. Zheng, H.; Wu, J., *J. Appl. Polym. Sci.* **2007**, *103*, 2564.

7. Liu, W.; Tian, X.; Cui, P.; Li, Y.; Zheng, K.; Yang, Y., *J. Appl. Polym. Sci.* **2004**, *91*, 1229.

8. Tian, X.; Ruan, C.; Cui, P.; Liu, W.; Zheng, J.; Zhang, X.; Yao, X.; Kangzheng; Li, Y., *J. Macromol Sci.* **2006**, *45*, 835.

9. Bikiaris, D.; Karavelidis, V.; Karayannidis, G., *Macromol. Rapid Commun.* **2006**, *27*, 1199.

10. Yang, Y.; Gu, H., *J. Appl. Polym. Sci.* **2006**, *102*, 3691.

11. Zheng, J.; Cui, P.; Tian, X.; Zheng, K., *J. Appl. Polym. Sci.* **2007**, *104*, 9.

12. Yang, Y.; Gu, H., *J. Appl. Polym. Sci.* **2007**, *105*, 2363.

13. Chung, S. C.; Hahm, W. G.; Im, S.; Oh, S. G., *Macromol. Res.* **2002**, *10*, 221.

14. Wu, T.; Ke, Y., *Polym. Degrad. Stab.* **2006**, *91*, 2205.

15. Wu, T.; Ke, Y., *Thin Solid Films* **2007**, *515*, 5220.

16. Koo, J. H., Polymer Nanocomposites Processing, Characterization, and Applications; McGraw-Hill: New York, **2006**.

17. Kim, G. M.; Michler, G. H., *Polymer* **1998**, *39*, 5689.

18. Kim, G. M.; Michler, G. H., *Polymer* **1998**, *39*, 5699.

19. Reynaud, E.; Jouen, T.; Gauthier, C.; Vigier, G.; Varlet, J., *Polymer* **2001**, *42*, 8759.

20. Liu, Y.; Kennard, C. H. L.; Truss, R. W.; Calos, N. J., *Polymer* **1997**, *38*, 2797.

21. Viana, J. C.; Mano, J. F.; Denchev, Z. Z.; Oliveira, M. J.; Cramez, M. C., *Mater. Sci. Forum* **2006**, 1583.

22. Efimov, A. V.; Shcherba, V. Y.; Bakeyev, N. F., *Polym. Sci. U.S.S.R.* **1991**, *33*, 568.

23. Todorov, L. V.; Martins, C. I.; Viana, J. C., *Solid State Phenom.* **2009**, *151*, 113.

24. Oultache, A. K.; Kong, X.; Pellerin, C.; Brisson, J.; Pezolet, M.; Prud'homme, R. E., *Polymer* **2001**, *42*, 9051.

25. Todorov, L. V.; Viana, J. C., *Int. J. Mater Forming* **2008**, *1*, 661.

26. Todorov, L. V.; Martins, C. I.; Viana, J. C., *J. Appl. Polym. Sci.* **2012**, *124*, 470.

27. Todorov, L. V. Multiscale morphology evolution of PET and its nanocomposites under deformation, PhD thesis, Institute of Nanostructures, Nanomodelling and Nanofabrication – I3N, University of Minho, Portugal URL: http://hdl.handle.net/1822/15904.

28. Todorov, L. V.; Martins, C. I.; Viana, J. C., *J. Appl Polym Sci.* **2011**, *120*, 1253.

29. Parravicini, L.; Leone, B.; Auriemma, F.; Guerra, G.; Petraccone, V.; Dino, G. D.; Bianchi, R.; Vosa, R., *J. Appl. Polym. Sci.* **1994**, *52*, 875.

30. Goschel, U., *Polymer* **1996**, *37*, 4049.

31. Todorov, L. V.; Martins, C. I.; Viana, J. C., *J. Appl. Polym. Sci.,* **2013**, *128*, 2884.

32. Goschel, U.; Deutschert, K.; Abetzt, V., *Polymer* **1996**, *37*, 1.

33. Stribeck, N., X-Ray Scattering of Soft Matter; Springer: Berlin, **2007**.

34. Ran, S.; Wang, Z.; Burger, C.; Chu, B.; Hsiao, B. S., *Macromolecules* **2002**, *35*, 10102.

35. Blundell, D. J.; MacKerron, D. H.; Fuller, W.; Mahendrasingam, A.; Martin, C.; Oldman, R. J.; Rule, R. J.; Riekel, C., *Polymer* **1996**, *37*, 3303.

36. Kawakami, D.; Ran, S.; Burger, C.; Fu, B.; Sics, I.; Chu, B.; Hsiao, S. B., *Macromolecules* **2003**, *36*, 9275.

37. Kawakami, D.; Hsiao, B. S.; Ran, S.; Burger, C.; Fu, B.; Sics, I.; Chu, B.; Kikutani, T., *Polymer* **2004**, *45*, 905.

38. Kawakami, D.; Ran, S.; Burger, C.; Avila-Orta, C.; Sics, I.; Chu, B.; Benjamin, S. H.; Kikutani, T., *Macromolecules* **2006**, *39*, 2909.

39. Takemori, M. T., *Adv. Polym. Sci.* **1990**, *91/92*, 263.

40. Shioya, M.; Kawazoe, T.; Okazaki, R.; Suei, T.; Sakurai, S.; Yamamoto, K.; Kikutani, T., *Macromolecules* **2008**, *41*, 4758.

41. Kobayashi, H.; Shioya, M.; Tanaka, T.; Irisawa, T., *Compos. Sci. Technol.* **2007**, *67*, 3209.

42. Kobayashi, H.; Shioya, M.; Tanaka, T.; Irisawa, T.; Sakurai, S.; Yamamoto, K., *J. Appl. Polym. Sci.* **2007**, *106*, 152.

43. Stribeck, N.; Nochel, U.; Fakirov, S.; Feldkamp, J.; Schroer, C.; Timmann, A.; Kuhlmann, M., *Macromolecules* **2008**, *41*, 7637.